Geophysical Journal International

Geophys. J. Int. (2014) doi: 10.1093/gji/ggu014

Geophysical Journal International Advance Access published February 13, 2014

Empirical evidence of local seismic effects at sites with pronounced topography: a systematic approach

Jan Burjánek, Benjamin Edwards and Donat Fäh

Swiss Seismological Service, Eidgenössische Technische Hochschule (ETH) Zürich, Sonneggstrasse 5, CH-8092 Zurich, Switzerland.
E-mail: burjanek@sed.ethz.ch

Accepted 2014 January 14. Received 2014 January 13; in original form 2013 June 17

SUMMARY

The recent growth of seismic monitoring networks allows for systematic studies of local seismic effects at sites with pronounced topography. We applied a terrain classification method to identify such sites within Swiss and Japanese networks and compiled a data set of high-quality earthquake recordings. As a number of recent studies have found local effects to be directional at sites with strong topographic features, polarization analysis of particle motion was performed and azimuthally dependent resonant frequencies were estimated. The same procedure was also applied for available ambient vibration recordings. Moreover, average residuals with respect to ground motion prediction models for a reference bedrock were calculated to estimate the average amplification or deamplification for each station. On one hand, observed amplifications are found to be tightly linked with ground motion directionality as estimated by polarization analysis for both earthquake and ambient vibration recordings. On the other hand, we found no clear relation between local topographic features and observed amplification, so the local subsurface properties (i.e. shear wave velocity structure) seem to play the key role and not the geometry itself.

Key words: Time-series analysis; Fourier analysis; Wavelet transform; Earthquake ground motions; Site effects; Wave propagation.

1 INTRODUCTION

The effects of surface topography geometry on seismic ground motions have been discussed for a long time, and have been the topic of many instrumental and numerical investigations over the last four decades. However, their complexity, combined with the limitations of both geophysical investigation techniques and numerical simulation, made it impossible until now to properly include such effects in earthquake hazard assessment and risk mitigation policies. The understanding and quantification of site effects is an important aspect of seismic hazard analysis, particularly in the case of detailed site-specific analyses for critical structures. An important question is therefore whether, despite the modelling and investigation complexity, it is important to consider the topographic component of site amplification when performing seismic hazard analysis. Moreover, site effects related to surface geometry are usually linked to coseismic landslides, which contribute significantly to earthquake damage (Marano *et al.* 2010).

A number of purely numerical studies have been produced, focusing mainly on the challenging task of introducing complex topography into wave propagation codes (e.g. Boore 1972; Bouchon *et al.* 1996; Moczo *et al.* 1997; Komatitsch & Vilotte 1998). Such simulations generally suggest an amplification of ground motion on mountain crests due to constructive interference of seismic waves within convex shapes, while at footslopes deamplification of ground motion is expected due to scattering at concave shapes. Amplification/deamplification factors of up to 2 are expected for very special cases (e.g. Assimaki *et al.* 2005; Lee *et al.* 2009), with the specific value depending on the geometry and on the reference site selection (e.g. Paolucci 2002; Maufroy *et al.* 2012). However, cases of pronounced amplification evident in strong ground motion recordings have been reported at sites with specific topographic features (e.g. Davis & West 1973; Tucker *et al.* 1984; Shakal *et al.* 1988; Spudich *et al.* 1996) while increased damage has been identified at such sites after earthquakes (e.g. Gazetas *et al.* 2002; Hough *et al.* 2010; McCrink *et al.* 2010). Although attempts have been made to explain such observations with the effect of the terrain geometry, these strong levels of observed amplification remain unexplained in most cases (e.g. Bouchon & Barker 1996; Lovati *et al.* 2011). It has turned out that the observed amplifications cannot be explained only by the geometry of the topography, and are instead tightly linked with the local subsurface structure, specifically the shear wave velocity (e.g. Paolucci *et al.* 1999; Assimaki *et al.* 2005; Graizer 2009; Glinsky & Bertrand 2011; Gallipoli *et al.* 2013). Nevertheless, the published observations present isolated case studies with different levels of investigations, thus it is difficult to find common conclusions.

Coseismic landslides are of great significance in seismic risk studies, and are sometimes related to the influence of the soil and rock conditions and the surface geometry on incident ground motion

(Sepúlveda *et al.* 2005). The seismic response of unstable rock slopes is not part of this paper, as we consider it as a very site-specific problem. The observed site effects on unstable rock slopes seem to be particular cases, for example, amplification factors may reach values of up to 30 over very short distances (Burjánek *et al.* 2010, 2012) and purely geometrical effects seem to be almost negligible (Moore *et al.* 2011).

In this paper, we follow a different strategy to previous studies. We do not focus on a single site, but rather perform a systematic study on a set of sites with pronounced topography. This is possible since the density of seismic networks has increased over recent years, with a number of stations located on pronounced topographic features. Moreover, homogeneous site characterization has been performed for various networks including geophysical investigation (e.g. KiK-net and K-NET in Japan, Swiss National Seismic Network, CHNet). We therefore present a systematic study of Swiss CHNet and Japanese KiK-net sites. A quantitative terrain classification of the sites was performed to select sites of interest in an objective way. The ground motion recordings collected at these selected sites were subsequently analysed. Average amplification functions with respect to ground motion prediction models for a reference rock were calculated to estimate frequency-dependent amplification and deamplification. Moreover, we analyse the directionality of ground motion since a number of observational studies have found directional site effects at locations with pronounced topography (e.g. Bonamassa & Vidale 1991; Spudich *et al.* 1996; Del Gaudio & Wasowski 2007; Burjánek *et al.* 2010, 2012; Massa *et al.* 2010; Pischiutta *et al.* 2010, 2011; Panzera *et al.* 2011). Thus, we propose the polarization analysis of particle motion as an additional element of the ground motion characterization.

2 DATA

2.1 Seismic data

A number of instrumented sites with complex topography were identified in Switzerland and Japan. These regions present ideal situations to systematically study effects at such sites. First, both Switzerland and Japan have rough topography and a relatively high density of seismic stations. Secondly, many of the Swiss permanent stations have a detailed site characterization including measured *S*-wave velocity profiles down to 30–100 m, and mean amplification functions relative to the Swiss reference profile are available for all stations (Fäh *et al.* 2009; Edwards *et al.* 2013). Shear wave velocity profiles are also available for all KiK-net stations down to at least 100 m. Finally, ground motion prediction models are available for both Japan and Switzerland with respect to precisely derived reference velocity profiles (Poggi *et al.* 2011, 2013). Both weak-motion earthquake and ambient vibrations recordings were collected for the Swiss network. Only earthquake recordings were available for the KiK-net stations.

2.2 Digital elevation model (DEM)

The 'Advanced Spaceborne Thermal Emission and Reflection Radiometer' (ASTER) 'Global Digital Elevation Model Version 2' (GDEM V2) was used to represent the terrain's surface. The model is available at no charge as a set of georeferenced images. The DEM accuracy, in terms of the standard deviation with respect to the reference model, is reported to be in the range of 7–14 m depending mainly on land cover (i.e. the DEM is less accurate in the areas covered by woods). The images are referenced by latitude/longitude (WGS84) with a posting interval of 1 arcsec, which is roughly 30 m for the areas of interest.

3 METHODS

3.1 DEM analysis

In order to characterize the surface geometry of a given site, we adopted a classification scheme proposed by Weiss (2001). The scheme is based on the so-called Topography position index (TPI), which is defined as a difference between the actual value of the elevation H at given location $[x, y]$ and mean elevation of the neighbouring area A:

$$TPI\,(x, y) = H\,(x, y) - \int_A H\,(x, y)\mathrm{d}S / \int_A \mathrm{d}S. \quad (1)$$

The area A should be centred at the point $[x, y]$. Both the size and the shape of the neighbouring area have to be defined in advance, depending on the specific application. In general, there is no constraint on both values. We use a square area for simplicity. The size of the area, however, presents a more fundamental issue. Surface topography has a self-affine nature (e.g. Turcotte 1997), so it is very difficult to define a general characteristic length scale. For this reason, the choice of scale depends on the specific use. For example, in our case, we are interested in ground motions in a characteristic frequency band (or wavelength) at a given site. Such a frequency band can be represented by a wavelength range, assuming a seismic velocity profile under the site. As these characteristic wavelengths are of principal interest, one should consider them in the selection of length scales for the topography classification. Unfortunately, since the seismic velocity structure is very variable in the uppermost part of crust and generally not known, it is impossible to define general wavelengths of interest for such seismological application. Moreover, the relation between seismic wavelengths and classification scales is not trivial and, for example, depend on the steepness of the slope.

Our final terrain classification follows Weiss (2001) and is based on the combination *TPI* and *Slope* values at given location. The *Slope* value is defined as a local steepest slope angle γ, that is, a magnitude of gradient:

$$\gamma\,(x, y) = \tan^{-1}\sqrt{\left[\frac{\partial H\,(x, y)}{\partial x}\right]^2 + \left[\frac{\partial H\,(x, y)}{\partial y}\right]^2}. \quad (2)$$

In particular, *TPI* at a particular location is compared to the standard deviation σ_{TPI} of the *TPI* over the entire region. The slope value is used to distinguish between flat areas and areas in the middle of a slope, both of which have TPI close to zero. The definition of the different classes is presented in Table 1.

Here, we briefly describe the technical details of the procedure, which are related to a specific DEM (ASTER GDEM in this case).

Table 1. Terrain classification.

Class number	Class name	TPI range	Slope
1	Valley	$\mathrm{TPI} \le -\sigma_{\mathrm{TPI}}$	-
2	Lower slope	$(-\sigma_{\mathrm{TPI}}, -0.5\sigma_{\mathrm{TPI}})$	-
3	Flat area	$(-0.5\sigma_{\mathrm{TPI}}, 0.5\sigma_{\mathrm{TPI}})$	Slope $\le 5^\circ$
4	Middle slope	$(-0.5\sigma_{\mathrm{TPI}}, 0.5\sigma_{\mathrm{TPI}})$	Slope $> 5^\circ$
5	Upper slope	$(0.5\sigma_{\mathrm{TPI}}, \sigma_{\mathrm{TPI}})$	-
6	Ridge	$\mathrm{TPI} \ge \sigma_{\mathrm{TPI}}$	-

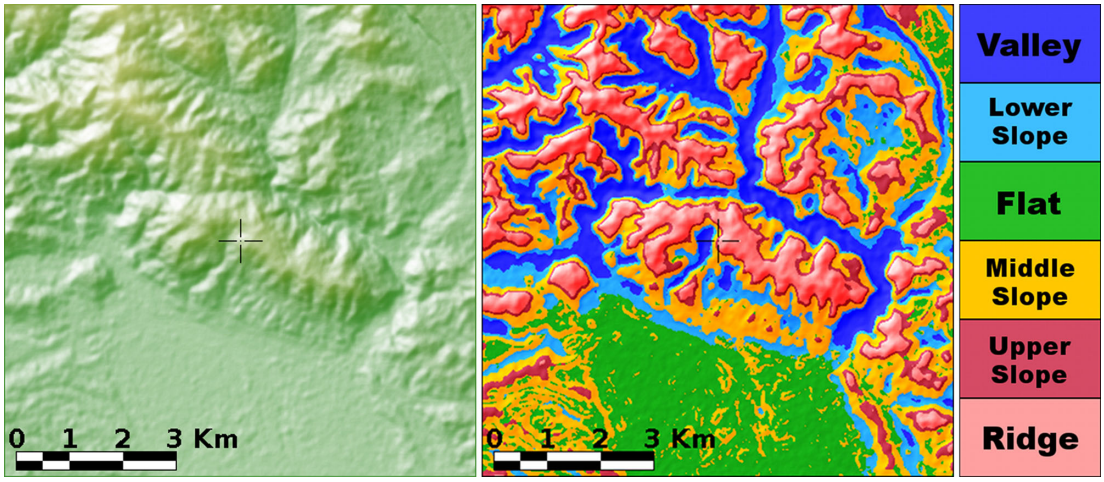

Figure 1. Digital elevation model (on the left-hand panel) and slope classification (on the right-hand panel). The black cross denotes the location of the seismic station. A spatial window of 1020 m was used in this example.

At first, a region of 500 × 500 arcsec surrounding the seismic station was cut out from the DEM, as the analysis of the complete DEM would result in heavy calculations. Secondly, the DEM was smoothed using a 3 × 3 pixel (approximately 90 × 90 m) moving average to avoid small-length scale artefacts in the DEM. Thirdly, since the ASTER GDEM is saved in the geographic coordinate system (WGS84) it is necessary to make a transformation to a Cartesian coordinate system to simplify the calculations of terrain parameters (*Slope*, *TPI*). Thus, the DEM was converted to Universal Transverse Mercator coordinate system. Finally, the area of 8 × 8 km surrounding the seismic station was cut out from the converted image. This procedure was performed for all 689 KiK-net locations. As the KiK-net network covers more or less uniformly the entirety of Japan, different terrain types are sampled: the Japanese terrain morphology is therefore well represented by the DEM subselection. By performing several tests, we found that the total area analysed is sufficient for a stable definition of the standard deviation σ_{TPI}, which is used for the terrain classification (see Table 1). An example of the terrain classification using ASTER GDEM is presented in Fig. 1 using a length scale of 1020 m for defining the area A. The influence of the selected length scale is presented later. The same procedure was applied for the station locations of CHNet. The value of standard deviation σ_{TPI} estimated for Japan was also applied for the Swiss sites to keep results consistent. Moreover, in case of Japan, almost 700 locations were analysed compared to 20 sites in Switzerland, thus σ_{TPI} estimated for Japan is more robust (i.e. a diversity of terrains was better sampled in Japan than in Switzerland).

3.2 Ground motion analysis

Several methods were applied to recorded ground motion. At first, particle motion analysis was applied to both recorded ambient vibration and earthquake recordings. Secondly, an earthquake spectral fitting procedure was utilized to isolate site effects.

3.2.1 Particle motion analysis

Several methods exist for the analysis of the directional site effects. Spudich *et al.* (1996) introduced directional site-to-reference spectral ratios (SRSRs) for the estimation of the relative amplification depending on both frequency and azimuth. This method has been widely applied (e.g. Pischiutta *et al.* 2010; Massa *et al.* 2010), however, it requires a reference station, which is not always available. Therefore, directional non-reference H/V spectral ratios (HVSRs) have been also applied in past studies (e.g. Del Gaudio & Wasowski 2007). Whereas HVSR has been commonly applied on both earthquake and noise recordings, SRSR has been primarily used with earthquake recordings. Nevertheless, the SRSR method can also be applied to noise recordings if it can be assured that the noise generating sources (for frequencies of interest) are far from the site with respect to the distance between the site and the reference station (Roten *et al.* 2006; Burjánek *et al.* 2012). In this work, we focus on the non-reference methods, as a reference station is not available for most of the sites.

Recently, Burjánek *et al.* 2010 introduced time–frequency polarization analysis (TFPA), which is based on the combination of complex polarization analysis (Vidale 1986) and the continuous wavelet transform (CWT). It can be viewed as a generalization of the directional HVSR method. Three polarization parameters are retrieved: (1) the azimuth of the major polarization axis, or strike, measured in degrees from north; (2) tilt of the major axis, or dip, measured in degrees downwards from the horizontal and (3) ellipticity, defined as the ratio between the length of the semi-minor and semi-major axes such that zero implies linear particle motion, while unity implies circular particle motion. All three polarization parameters vary with both time and frequency. Usually, we assume that observed ambient vibrations are quasi-stationary (i.e. noise properties do not change systematically on the timescale of the experiment—typically a few hours), and analyse the relative occurrence of polarization parameters. In particular, histograms of polarization parameters are constructed over time for each frequency. Polar plots are then adopted for the presentation of results, which illustrate combined angular and frequency dependence. While directional HVSR can be used to estimate just the polarization azimuth (orientation in horizontal plane), the TFPA method also provides information on the inclination of the particle motion (dip). Moreover, the use of CWT maintains optimum time–frequency resolution, which can be smoothly regulated through adjustment of the mother wavelet.

We found that the observed histograms of strike and dip can be fit by the Wrapped Cauchy distribution for given frequency. The Wrapped Cauchy distribution is a circular distribution, that is, used

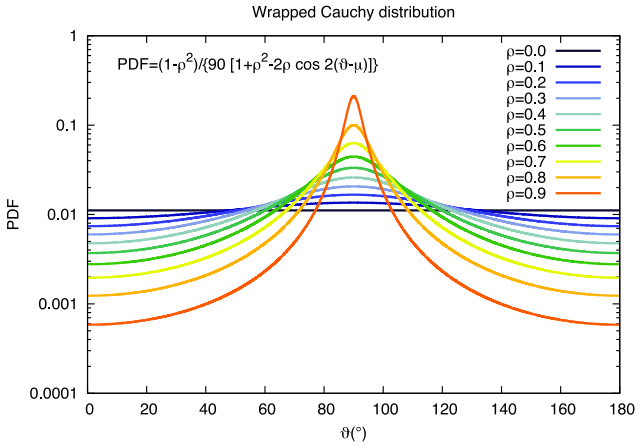

Figure 2. The Wrapped Cauchy distribution is used for the description of strike and dip angles. It is characterized by mean μ and concentration parameter ρ. The presented examples have all 180° period, mean $\mu = 90°$ and show the influence of concentration ρ (different colours).

to describe periodic quantities (like angles). It is a symmetric distribution and is characterized by mean and concentration value. An example of Wrapped Cauchy distributions is provided in Fig. 2. The concentration parameter ρ measures the scatter. While $\rho = 0$ results in the uniform distribution (see Fig. 2), $\rho = 1$ results in the Dirac delta function. Both mean and concentration can be estimated for a given frequency, for example, by applying a maximum likelihood method. This allows for a quantitative analysis of polarization analysis results. In other words, the frequency-dependent level of directionality is mapped to the frequency-dependent concentration value ($\rho = 0$ signifies no directionality, while $\rho \approx 1$ means completely directional). Note that the concentration value is independent of the ellipticity value defined earlier—motion can be polarized most of the time (i.e. low ellipticity), but the orientation of this polarized motion can vary in time (i.e. low concentration).

3.2.2 *Spectral analysis of earthquake recordings*

Elastic amplification functions and near-surface attenuation terms (κ_0, Anderson & Hough 1984) were determined for the studied sites through the empirical spectral modelling approach of Edwards *et al.* (2013). Combined, these terms form the anelastic amplification function describing the influence of the upper soil or rock layers on the wavefield for each site. The employed method robustly isolates the site contribution through a multiple stage non-linear regression. The inversion is stabilized through a parametric description of the source and path: a Brune (1970) ω^2 point source model is assumed for small to moderate ($M < 6$) events at sufficient distance, while intrinsic and geometrical attenuation is accounted for using frequency-dependent exponential decay and frequency-independent $1/R^{\lambda}$ type spreading, respectively. Moment magnitudes, independently determined by the United States Geological Survey (USGS) for Japan or the Swiss Seismological Service for Switzerland are used to decouple the trade-off between source and site. The use of non-parametric site terms allow for the consideration of 2- or 3-D effects and the influence of surface waves. Through this approach, consistently observed site-specific effects are extracted relative to a reference model (Poggi *et al.* 2011, 2013). Exhaustive description of the method and extensive testing, showing consistency with existing methods such as 1-D SH and SRSRs, can be found in Edwards *et al.* (2013).

4 RESULTS

4.1 DEM analysis

DEM analysis was performed to characterize the stations' locations. The key issue of the DEM analysis is the selection of the appropriate *scale*, represented by the size of the spatial window which defines *TPI*. As the characteristic wavelengths are generally not known for the investigated sites, a multiscale analysis is required. In other words, several windows of different size (area A in Eq. 1) are applied, so the classification is not a single index, but a set of numbers, depending on the scale (size of the window). As a result, such classifications cannot be directly linked to seismic amplification unless the relation to seismic wavelengths is known. This is generally a difficult task due to the limited knowledge of the subsurface velocity structure and potential 3-D wave propagation effects. The influence of the selected *scale* is presented in Fig. 3. As expected, except for flat areas, on the very top of sharp crests and at the very bottom of sharp V-shaped valleys (i.e. for strictly self-similar structures), site classification strongly depends on the scale. Thus, the classification of all Japanese and Swiss sites was performed with five different scales (120, 220, 500, 1020 and 2020 m). By scale we always mean

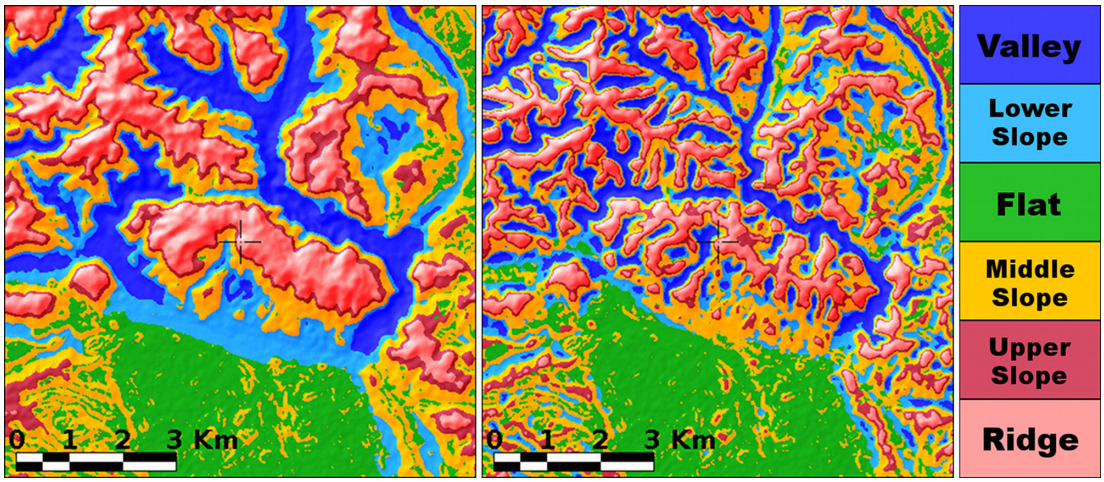

Figure 3. An example of the slope classification's dependence on the *scale*. Spatial windows of 2020 m (on left-hand panel) and of 500 m (on right-hand panel) were utilized in classification. The DEM is the same as in the Fig. 1.

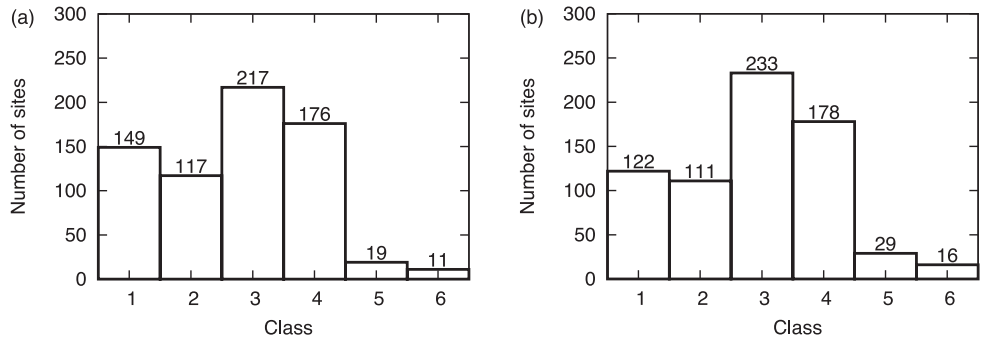

Figure 4. Distribution of the KiK-net sites according to terrain classes: (a) at 1020 m scale; (b) at 500 m scale. The definition of the classes is in the Table 1.

the size of square spatial window (area A in Eq. 1). The distribution of the KiK-net sites according to terrain classes at 1020 and 500 m is plotted in Fig. 4. A weak correlation was found between the different scales, which decreases with increasing scale ratio. For example, most of the ridge sites identified at scale 2020 m are also identified as ridges using the 1020 m scale. We focus here on the sites classified as ridges, since the amplification effects due to topography are expected to be strongest at these locations (e.g. Lee *et al.* 2009; Maufroy *et al.* 2012). Moreover, the classification of the ridge is less scale dependent, especially in the vicinity of mountain crests (see Fig. 3). Nevertheless, the number of such sites naturally still increases with decreasing scale. We limited our study to sites identified as ridges only at scales of either 1020 or 2020 m for which we can expect effects over a wide frequency band. Assuming a hill's height of a few hundred metres and shear wave velocities in range of 1500–3000 m s^{-1}, which are usually considered in numerical studies of topographic site effects, the lower limit of this range is 0.5–2 Hz. In particular, we decided to study only sites with the most pronounced topographic features in mountainous regions to reduce the analysis to fewer sites, but with deeper insight. The selected 25 KiK-net and Swiss sites are listed in Table 2 together with available site information.

4.2 Ground motion analysis at selected sites

In case of the Swiss stations, polarization analysis was performed on both earthquake and ambient vibration recordings. Windows of 2 hr of ambient vibration recordings were cut out from continuous recordings for each station. These time windows usually start after midnight to prevent (as much as possible) the recording of human activity. Recordings were checked visually for any transients and only stationary signals were processed. In addition, a number of earthquake recordings were selected for each site (20 events on average). These are recordings of local events (epicentral distance less than 50 km, local magnitudes M_L in range of 2–4) with good signal-to-noise ratio. Seismograms were merged to a single three-component time-series and processed in the same way as ambient vibrations. Complete seismograms entered the analysis; no windowing was applied, so that recordings include few seconds of ambient noise at the beginning. However, the duration of these ambient vibrations is small compared to duration of the earthquake ground motion.

A comparison of the concentration of the strike angle for four representative sites (FLACH, AIGLE, BALST and HASLI) is shown in Fig. 5. At station FLACH, the ground motion is directional (a peak in concentration of the strike angle exists) at 4.5 Hz. In this case, a good agreement between the noise and earthquake recordings was also apparent. A similar agreement was found for station AIGLE, where the ground motion becomes directional at 3.5 Hz, however, other peaks in concentration also appear in the case of ambient vibrations (2.3, 25 Hz). These two peaks likely have an industrial origin. The stations FLACH and AIGLE represent sites with directional site response. No peaks in concentration are observed at station BALST for both earthquake and ambient vibration recordings, while at station HASLI one can see only a peak in concentration close to 16.5 Hz. This peak has a likely industrial origin (probably related to AC frequency of 16.7 Hz of the Swiss rail network which is operating less than 500 m from the site). The stations BALST and HASLI represent sites with an isotropic site response. Due to the similar results obtained for earthquake recordings and ambient vibrations, a simple ambient vibration measurement can be applied to assess possible amplification effects at rock slope sites (see below). Nevertheless, industrial peaks represent a general problem in ambient vibration surveys. Moreover, such ground motion generated from one mostly harmonic source is observed to be usually strongly directional, thus can easily bias our polarization analysis. A careful analysis of ambient vibration time-series is therefore necessary to prevent confusing the directional site response with the directionality of strong industrial sources. Since such sources usually have very narrow band spectra, it is possible to recognize them through analysis of the power spectral densities. Furthermore, since the ambient vibrations in this study were recorded during the night, and have relatively long duration (2 hr), the results presented here represent a rather good end case.

Only earthquake recordings are available at KiK-net stations. For the polarization analysis, the data selection includes both regional and local events (60 events per site on average; epicentral distance less than 100 km; magnitude M_{JMA} in range of 2–6.5). Both surface and borehole recordings were analysed.

The empirical spectral modelling approach was performed for earthquake recordings on both KiK-net and Swiss stations. The earthquake recordings are not necessarily the same as for the polarization analysis, since there are different selection criteria for the ground motion in case of the spectral fitting (e.g. sufficient number of stations per event, point source approximation, S-wavefield only). We are not interested in the source properties in this study, so only the non-parametric site term is of our interest. This site term represents the frequency-dependent relative amplification with respect to a precisely derived reference profile (Poggi *et al.* 2011, 2013) and can be viewed as an analogue to the SRSR (Edwards *et al.* 2013). Amplification functions were not estimated for the sites EHMH08, KGSH12 and CHBH16, because of a limited amount of suitable recordings at these sites.

Table 2. Site characterization of the sites located on ridges. EC8 classification is based on Vs30 values. The colour of the field in the sixth column distinguishes the level of directionality: strong directionality (red), weak directionality (green), no directionality + no amplification (blue) and not classified (white).

CODE	Borehole depth (m)	Vs100 (m/s)	Vs30 (m/s)	EC8 Class	f_0^{ampl} (Hz) / f_0^{pol} (Hz)	Lithology
AICH07	201	1001	428	B	-	Gravel and Sand (14 m), Gneiss
NARH01	99	792	338	C	-	Slate
WKYH08	112	590	344	C	1.7 / 1.8	Hard weathered sandstone (27 m), Sandstone
KMMH10	300	712	463	B	-	Talus deposit (11 m), Sandstone, Shale
NGSH06	200	1803	1421	A	-	Strongly weathered green schist (7 m), Schist
OITH10	100	1366	837	A	-	Clay (4 m), Sandstone / Shale
MYGH09	100	560	358	C	13.5 / 16.0	Sand+Gravel (6 m), Ash breccia and Curd / Silt
EHMH08	100	729	364	B	-	Gravel clay mixed (18 m), Green and red shale rock
KGSH12	150	977	452	B	-	Aplite (25 m), Granodiorite
YMGH15	110	1120	549	B	7.1 / 6.3	Weathered crystalline schist (16 m), Sandy / Pelticschists
KNGH20	106	503	273	C	-	Soil (2 m), Tuff, Conglomerate
SZOH34	118	699	430	B	6.4 / 6.0	Loam (13 m), Lapilli tuff, Sandstone / Conglomerate / Basaltic rock
SZOH35	300	324	158	D	2.1 / 1.5	Sand and Gravel (13 m), Rocks / Basaltic rock, Ash breccia and Curd
CHBH16	2003	542	361	B	-	Mudstone / Sandstone interbedded (140 m)
ACB	-	-	658	B	-	Station in weathered rock (Jurassic sediments), about 10 m below the surface. Surface material: gravels
AIGLE	-	-	1243	A	-	Station about 20 m below the surface in rock: Jurassic (Malm) sediments, limestones
BALST	-	-	1348	A	-	Rock: Jurassic (Malm) sediments, limestone with karst formations
FLACH	-	-	610	B	5.6 /4.8	Lower Freswater Molasse (USM, Aquitanien): layered sandstones, marl and conglomerates; Surface material: unconsolidated, loose scree.
HASLI	-	-	1603	A	-	Rock: Jurassic (Malm) sedimentshard, massive limestone
MUO	-	-	1086	A	-	Lower Cretaceous limestone
PLONS	-	-	1810	A	-	Permian sedimentary rock (Verrucano)
SLE	-	-	686	B	-	Mesozoic sediment ridge (limestone and marl)
STEIN	-	-	387	B	-	Rock composed of sediments of the Upper Freshwater Molasse (OSM, Miocene). Surface material: loose sediments.
SULZ	-	-	1028	A	-	Mesozoic sediment ridge (massive limestones)
WILA	-	-	683	B	4.2 /4.1	Unsorted conglomerates (Nagelfluh) (Upper Freshwater Molasse)

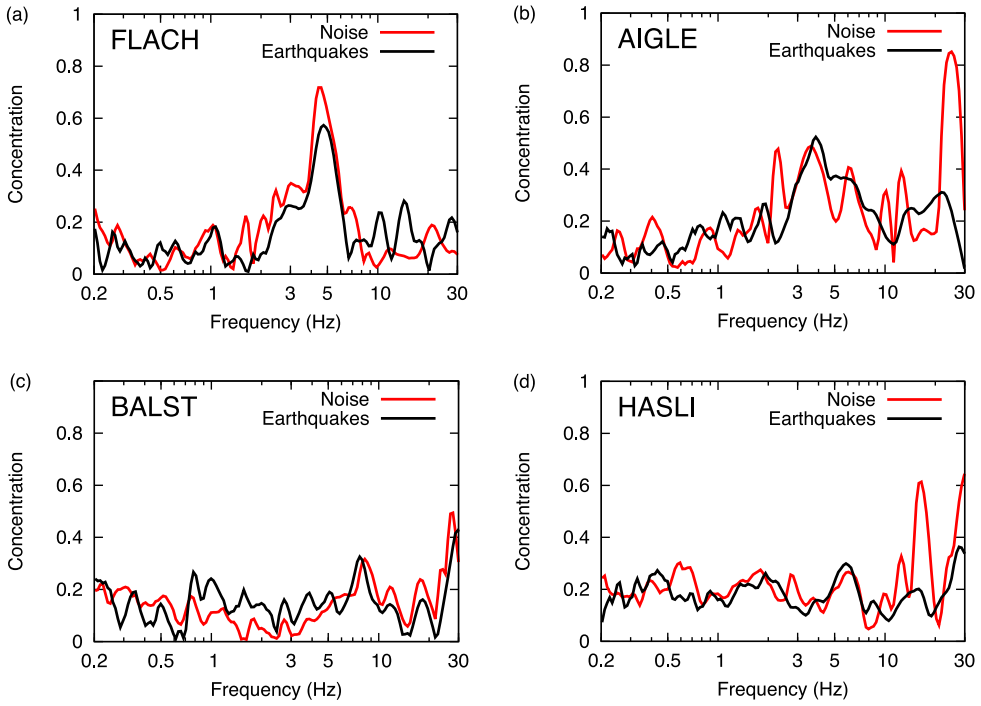

Figure 5. Concentrations of polarization strike angles as a function of frequency. Comparison of the polarization analysis for earthquakes and ambient vibrations—typical situations: (a) a station with ground motion directionality and good agreement; (b) a station with ground motion directionality and with peaks in the curve obtained from ambient vibrations caused by anthropic sources; (c) a station without ground motion directionality and good agreement and (d) a station with ground motion directionality and with peaks in the curve obtained from ambient vibrations caused by anthropic sources.

The results for all sites are provided in the Supporting Information. We summarize here the main findings by presenting results for two representative sites. At first, results for the Swiss site BALST are presented in Fig. 6. Station BALST is a hard rock site (with traveltime average shear wave velocity in the upper 30 m (Vs30) of 1348 m s^{-1}) located just at the edge of a 300-m high limestone cliff (Fig. 6a). A topographic effect is expected here. However, we do not observe any systematic amplification at this site (Fig. 6c). Moreover, we observe almost no directionality of the ground motion (Fig. 6b). The concentration of the strike angle remains low (Fig. 6c) at all frequencies, and the ellipticity follows more or less the constant value of about 0.4 (Fig. 6d). Results for a KiK-net site YMGH15 are presented in Fig. 7. Station YMGH15 is located on a 100-m high hill (Fig. 7a). The site has been classified as EC8 class B with Vs30 = 549 m s^{-1}, while the borehole lithology log shows layers of weathered schist. The amplification curve at this site has a peak at 6 Hz (Fig. 7c), and the amplification reaches factor of 4 with respect to the reference profile. Moreover, at the same frequency of 6 Hz the strike angle concentrates at 175° (Fig. 7b) and the ellipticity drops below 0.1 (Fig. 7d). The concentration of the strike at 6 Hz is relatively high, reaching 0.7 (Fig. 7c). Site YMGH15 therefore represents a site with a strong directional site effect.

The strike concentration and ellipticity mode curves for all sites are presented in Fig. 8. Sites which have been assigned Eurocode 8 soil class A (EC8 A, see Table 2) are distinguished by different colour from the remaining sites. In case of EC8 A sites, the ellipticity mode curves are flat and remain in the range 0.3–0.4 (black curves, Fig. 8). The strike concentrations for the EC8 A sites remain below 0.3 (black points, Fig. 8), except at Swiss sites AIGLE and MUO. On the other hand, most of the other sites (non-EC8 A) present different local minima in their ellipticity curves: dropping down to 0.1 (red curves, Fig. 8). Also concentrations of the strike reach higher values (up to 0.7) with respect to EC8 A sites (red points, Fig. 8). We define three levels of directional site effects: (1) strong directional site effect (clear peak in strike concentration >0.4); (2) weak directional site effect (clear peak in strike concentration ≈0.3–0.4) and (3) no directional site effect (no clear peaks in strike concentration <0.3). We also take into account the existence of local minima in ellipticity. A strike concentration of 0.4 means that the preferential direction is observed approximately five times more frequently than the perpendicular one, that is, clear directionality. Strike concentrations below 0.3 (still the preferential direction is three times more frequent) are difficult to interpret, as the ellipticity does not show any local minima for most of the cases, that is, particle motion is far from linear. The results of such directionality classification are presented in Table 2 (colour code of the sixth column). Although such a classification can be considered arbitrary (the border between weak and non-existing directional site effects is especially weak, e.g. OITH10, AICH07), it clearly highlights the link between strong amplification and ground motion directionality.

Finally, we noted that the frequency of the fundamental peaks (f_0) in the amplification curves correlates with the frequencies where the ground motion becomes directional (e.g. Fig. 7c). Thus, we manually picked and compared the frequencies of the peaks in amplification functions and strike concentration functions for non-EC8 A sites showing strong peaked directionality (see Table 2). The result of this comparison is presented in Fig. 9. The two measures of f_0 correlate very well. We do not provide any pick for the station NARH01, as the amplification function presents only a very broad peak (width of 10 Hz). We do not have any explanation for such behaviour, since it would require detailed site-specific analysis. Moreover, we do not identify any correlating peaks at Swiss stations STEIN and SLE. We also do not provide any interpretation for the sites with weak directional effects (see Table 2), since we could

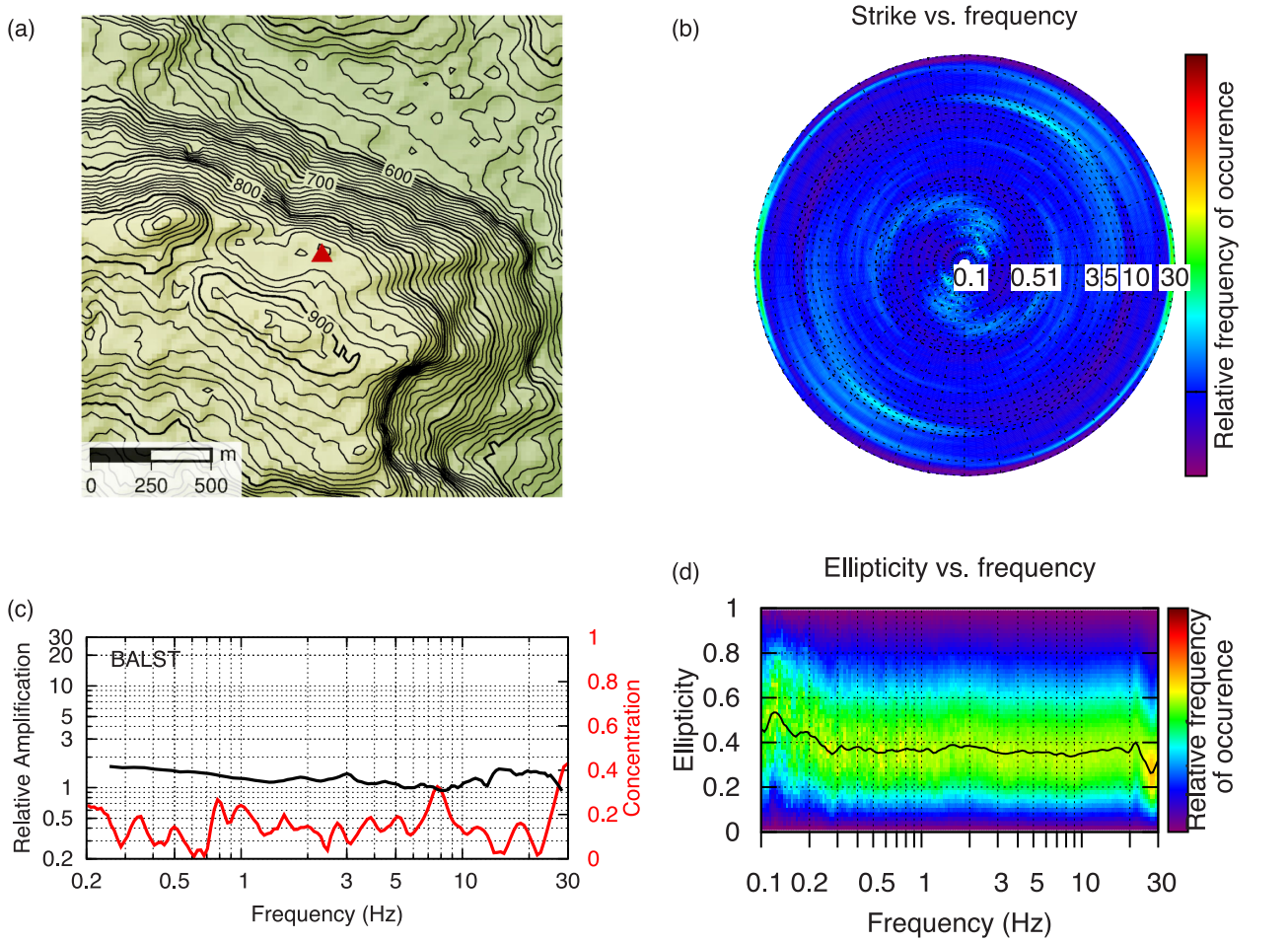

Figure 6. An example of a site with no site effect (Station BALST): (a) geometry of the terrain (based on Swiss Topo LIDAR swissALTI3D DEM, contour lines placed for every 10 m) and location of the station (red triangle); (b) distribution of the strike angle; (c) concentration versus amplification and (d) distribution of the ellipticity.

not simply identify other common features. Nevertheless, some of the weak peaks in the strike concentration seem to be related to an amplification peak at these sites, but not always.

5 DISCUSSION

We briefly summarize and discuss our observations. The rock sites (EC8 class A) with pronounced topography studied in this paper do not, on average, exhibit any systematic amplification. In particular, we do not observe any systematic residuals with respect to the reference ground motion prediction model nor any directionality of the motion. Nevertheless, the pure effects of surface geometry are usually reported to be source-dependent (especially with respect to the source location—e.g. Lee *et al.* 2009; Maufroy *et al.* 2012), so they might be averaged out in our amplifications functions. On the other hand, the rest of the sites (non-EC8 class A) present systematic frequency-dependent amplifications with respect to the two reference ground motion models (the reference ground model for Japan and Switzerland is not the same). Moreover, these observed site effects are found to be directional, that is, ground motion vibrates in specific directions. This directionality is observed in the both ambient vibration and earthquake recordings, thus seems to be source-independent. Although the distribution of backazimuths is not optimum at all sites in case of earthquakes recordings, the observed directionality cannot be linked to the source properties. To demonstrate this, we compare the results of the polarization analysis for the borehole and surface recordings at KiK-net sites in Fig. 10. The borehole recordings show consistently frequency-independent ellipticity (black curves, Fig. 10), and low concentration (<0.2) of the strike angle (black points, Fig. 10). So the directionalities diminish in the borehole recordings. The results for the borehole recordings are strikingly similar to the surface recordings of the hard rock sites.

Two Swiss stations (AIGLE and MUO) stick out slightly from the described scheme. Station AIGLE represents a peculiar case. It has relatively high Vs30 of 1243 m s^{-1}, but presents directionality and deamplification in the same frequency band with respect to the reference model. We do not have any explanation at the moment. However, the station is located in a bunker about 20 m below the surface and it might be that the station is influenced by this construction. Station MUO also presents a specific site response. In particular, the ground motion is polarized and directional at 1.5 Hz, and the high-frequency ground motion is remarkably attenuated. The site can be potentially unstable, since it carries similar signs at previously studied unstable rock slopes (Burjánek *et al.* 2010, 2012). Moreover, the *S*-wave velocity measurements characterizing this site were not taken exactly at the location of the seismic station, but tens of metres away. Thus, taking into account rapid variation of the subsurface structures within unstable rock slopes, the true velocity at site could be different. On the other hand, some non-EC8

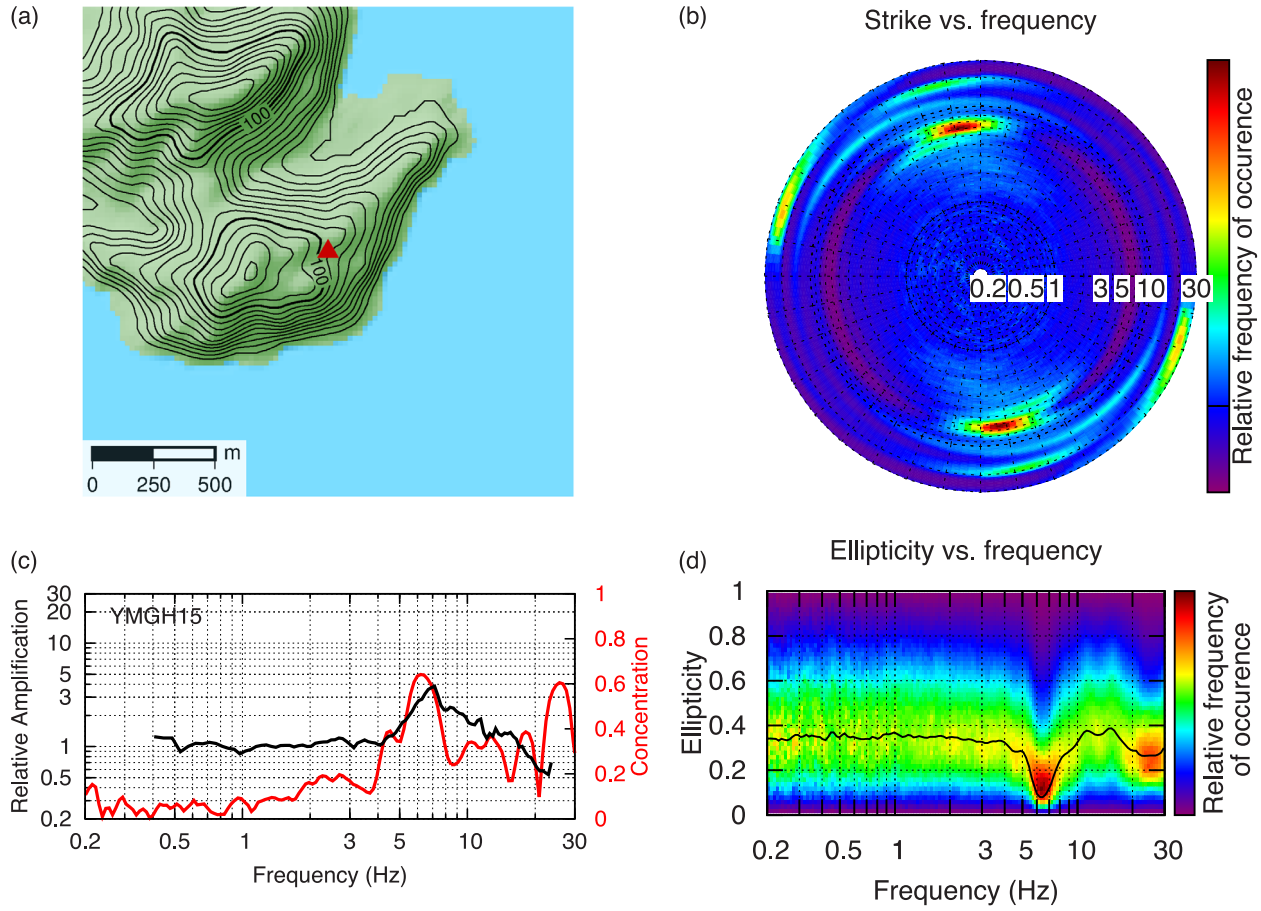

Figure 7. An example of a site with relatively strong site effect (Station YMGH15): (a) geometry of the terrain (based on ASTER GDEM, contour lines placed for every 10 m) and location of the station (red triangle); (b) distribution of the strike angle; (c) concentration versus amplification and (d) distribution of the ellipticity.

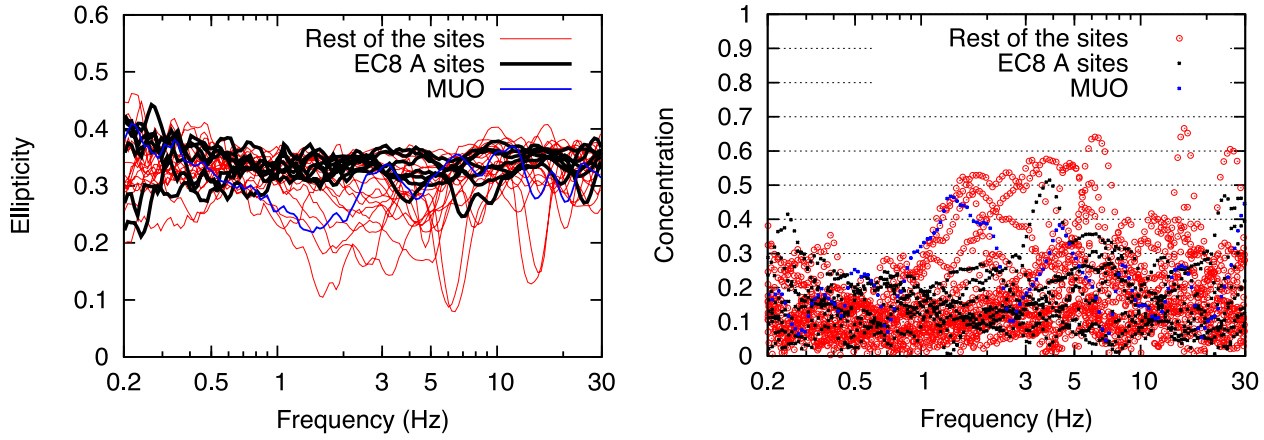

Figure 8. Comparison of the polarization analysis for station MUO (blue), EC8 class A stations (black) and rest of the stations (red) at KiK-net and Swiss sites. Modes of the ellipticity distributions are plotted on the left-hand plot, whereas concentrations of the strike angle are on the right-hand plot.

A sites show just weak amplification (e.g. STEIN and SLE). For example, station STEIN is classified as EC8 B site where class B refers to the location of the station several metres below the ground surface in rock and Vs30 = 383 m s^{-1} that refers to the free surface. No strong amplification and no directionality of ground motion are observed. This might be explained by station's location below the ground surface.

Finally, we have not identified any link between the surface topography and the observed response at studied 25 sites. Observed amplifications differ by factor of 20 for some site couples with comparable topography: a large difference with respect to expected ground motion variability due to surface geometry only (factor of 2, e.g. Lee *et al.* 2009). Therefore, the amplification is controlled in first place by the subsurface velocity structure. Although the effect

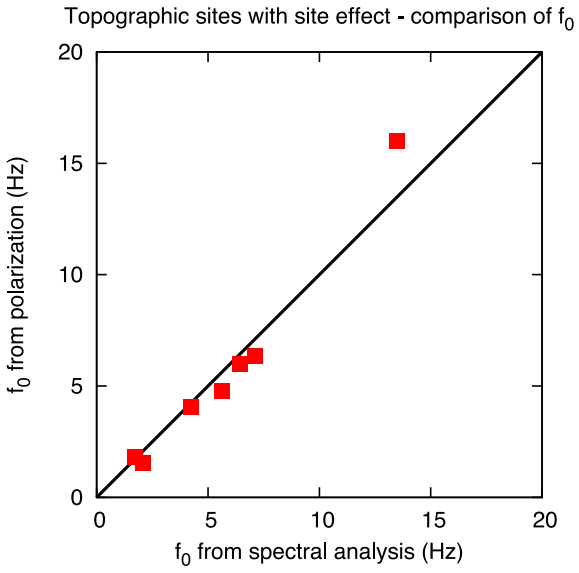

Figure 9. Fundamental frequencies picked from the amplification obtained from spectral fitting and from the polarization analysis. This assessment has been done for sites with clear directionality. The picks are presented in the Appendix S1.

of geometry is present, it cannot be simply decoupled from the site response. The observed directionality cannot be easily related to the terrain characteristics (e.g. aspect angle). Moreover, all terrain characteristics are scale-dependent, and thus strongly non-unique, omitting the subsurface velocity structure. Any future seismic site characterization of locations with complex geometry must have to account for the subsurface velocity structure. It is interesting that some of sites can be identified as outcropping rock sites looking at the borehole lithology log (e.g. WKYH08, KGSH12, NARH01 and YMGH15), however, the Vs30 values correspond to sediment sites. This shows the importance of the shear wave velocity measurements even at the rock outcrops. Nevertheless, all complexities mentioned in the previous paragraph suggest that observed site effects cannot be addressed just by simplified site classes (even based on Vs30 measurement). On the other hand, the response of the site can be evaluated quickly through passive seismic measurements, for example, by ambient vibration surveys. In particular, sites presenting no polarization or directionality of ground motion are likely subjected, if at all, to weak site effects. On the other hand, strong site effects can be expected in the case of observations of polarized and directional ground motion.

6 CONCLUSIONS

Strong systematic amplification observed at sites with pronounced topography presented in this study is controlled by subsurface structure, rather than shape of the topography. The pure effects of surface geometry might be observed only at hard rock sites where the amplification due to the subsurface structure does not dominate the wavefield. Although, based on our observation, such effects do not seem to result in systematic amplification nor deamplification, they might appear for specific source locations. The subsurface structure was found to be variable under the studied sites: even sites with rock outcrops presented a strong gradient of the shear wave velocity with depth. Thus, the seismic hazard estimate at sites with pronounced topography requires a detailed knowledge of the subsurface; especially shear wave velocity structure and internal structure, not only in case of instable rock slopes (Burjánek *et al.* 2011). Studies based exclusively on the terrain topography have almost no chance to capture the site effects correctly. It is also impossible to define characteristic wavelengths from the terrain only, since the surface topography has a self-affine nature.

The observed amplifications are correlated with ground motion directionality. Although a unique physical mechanism has not been discovered yet, ground motion directionality can be viewed as an indication of strong site effects. Since such directionality is also observed in a consistent way in the ambient vibration wavefield, noise measurements could therefore be used in the future for a quick characterization of topographic sites.

In terms of seismic hazard, this study suggests that efforts should be concentrated on modelling amplification due to subsurface structure rather than topographical effects. An important conclusion of this study is that the significance of amplification at a given site can be predicted at low cost through non-invasive polarization analysis of the ambient noise wavefield. Although such approaches are common in microzonation studies using classical HVSR approaches, the improved TFPA approach of Burjánek *et al.* 2010 can provide further information as to the likelihood of amplification phenomena occurring at a given site, even before more complex array–based approaches are undertaken. For instance, in the case of flat HVSR, without directionality or ellipticity (all of which are obtained using a single sensor), we can assume that site effects will not be

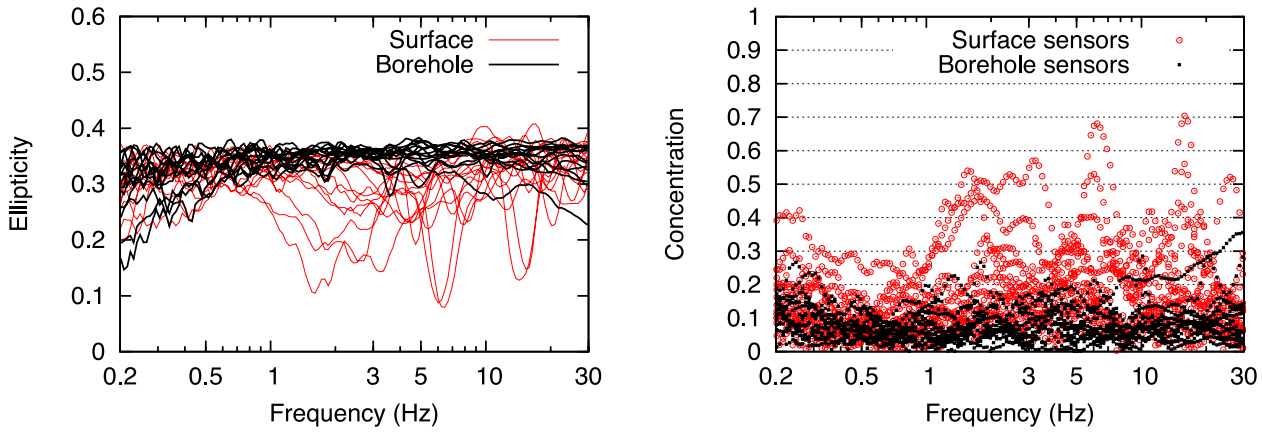

Figure 10. Comparison of the polarization analysis for surface (red) and borehole instruments (black) at KiK-net sites. Modes of the ellipticity distributions are plotted on the left-hand plot, whereas concentrations of the strike angle are on the right-hand plot.

significant, while in the case that one or more of these indicators shows a peak, that strong amplification may affect the site.

Ultimately, we do not state that the geometry of the surface has no effect on the ground motion. A successful prediction of the local response of sites with pronounced topography has an origin in the availability of a reliable shear wave velocity model representative of the site (i.e. a measured one). Detailed numerical modelling can subsequently reveal the joint effect of surface geometry and subsurface structure. The conclusions of this study are based just on analysis of 25 sites, so the further studies are required together with more physical insight based on numerical modelling.

ACKNOWLEDGEMENTS

We are indebted to Vera Pessina for helpful discussions and suggestions on the DEM classification. We thank Marco Stupazzini, and an anonymous reviewer for constructive comments and helpful suggestions. We thank the National Research Institute for Earth Science and Disaster Prevention, Japan (NIED) for making waveform and velocity profile KiK-net data available. This research is part of the EU project NERA (Network of European Research Infrastructures for Earthquake Risk Assessment and Mitigation, task JRA1—'Waveform modelling and site coefficients for basin response and topography'). The study is also funded in part by the Swiss Federal Nuclear Safety Inspectorate (ENSI). Wavelet software used in the polarization analysis was provided by C. Torrence and G. Compo, available at http://paos.colorado.edu/research/wavelets/.

REFERENCES

Anderson, J.G. & Hough, S.E., 1984. A model for the shape of the Fourier amplitude spectrum of acceleration at high-frequencies, *Bull. seism. Soc. Am.,* **74,** 1969–1993.

Assimaki, D., Gazetas, G. & Kausel, E., 2005. Effects of local soil conditions on the topographic aggravation of seismic motion: parametric investigation and recorded field evidence from the 1999 Athens earthquake, *Bull. seism. Soc. Am.,* **95,** 1059–1089.

Bonamassa, O. & Vidale, J.E., 1991. Directional site resonances observed from aftershocks of the 18th October 1989 Loma Prieta earthquake, *Bull. seism. Soc. Am.,* **81,** 1945–1957.

Boore, D.M., 1972. A note on the effect of simple topography on seismic SH waves, *Bull. seism. Soc. Am.,* **62,** 275–284.

Bouchon, M. & Barker, J.S., 1996. Seismic response of a hill: the example of Tarzana, California, *Bull. seism. Soc. Am.,* **86,** 66–72.

Bouchon, M., Schultz, C. & Toksoz, M., 1996. Effect of three-dimensional topography on seismic motion, *J. geophys. Res.,* **101,** 5835–5846.

Brune, J.N., 1970. Tectonic stress and spectra of seismic shear waves from earthquakes, *J. geophys. Res.,* **75,** 4997–5010.

Burjánek, J., Gassner-Stamm, G., Poggi, V., Moore, J.R. & Fäh, D., 2010. Ambient vibration analysis of an unstable mountain slope, *Geophys. J. Int.,* **180,** 820–828.

Burjánek, J., Moore, J.R., Gassner-Stamm, G. & Fäh, D., 2011. Seismic response of unstable mountain rock slopes: topographic site effect? in *Proceedings of the 4th IASPEI/IAEE International Symposium: Effects of Surface Geology on Seismic Motion,* In CD, University of California Santa Barbara, CA.

Burjánek, J., Moore, J.R., Yugsi-Molina, F.X. & Fäh, D., 2012. Instrumental evidence of normal mode rock slope vibration, *Geophys. J. Int.,* **188,** 559–569.

Davis, L.L. & West, R., 1973. Observed effects of topography on ground motion, *Bull. seism. Soc. Am.,* **63,** 283–298.

Del Gaudio, V. & Wasowski, J., 2007. Directivity of slope dynamic response to seismic shaking, *Geophys. Res. Lett.,* **34,** L12301, doi:10.1029/2007GL029842.

Edwards, B., Michel, C., Poggi, V. & Fäh, D., 2013. Determination of site amplification from regional seismicity: application to the Swiss National Seismic Networks, *Seismol. Res. Lett.,* **84,** 611–621.

Fäh, D. *et al.*, 2009. Determination of site information for seismic stations in Switzerland, Swiss Seismological Service Technical Report: SED/PRP/R/004/20090831, for the Swissnuclear Pegasos Refinement Project.

Gallipoli, M.R., Bianca, M., Mucciarelli, M., Parolai, S. & Picozzi, M., 2013. Topographic versus stratigraphic amplification: mismatch between code provisions and observations during the L'Aquila (Italy 2009) sequence, *Bull. Earthq. Eng.,* **11,** 1325–1336.

Gazetas, G., Kallou, P.V. & Psarropoulos, P.N., 2002. Topography and soil effects in the M-S 5.9 Parnitha (Athens) Earthquake: The case of Adames, *Natural Hazards,* **27,** 133–169.

Glinsky, N. & Bertrand, E., 2011. Numerical study of topographical site effects by a discontinuous finite element method, in *Proccedings of the 4th IASPEI/IAEE International Symposium: Effects of Surface Geology on Seismic Motion,* In CD, University of California Santa Barbara, CA.

Graizer, V., 2009. Low-velocity zone and topography as a source of site amplification effect on Tarzana hill, California, *Soil Dyn. Earthq. Eng.,* **29,** 324–332.

Hough, S.E. *et al.*, 2010. Localized damage caused by topographic amplification during the 2010 *M*7.0 Haiti earthquake, *Nature Geosci.,* **3,** 778–782.

Komatitsch, D. & Vilotte, J.P., 1998. The spectral-element method: an efficient tool to simulate the seismic response of 2D and 3D geological structures, *Bull. seism. Soc. Am.,* **88,** 368–392.

Lee, S.J., Chan, Y.C., Komatitsch, D., Huang, B.S. & Tromp, J., 2009. Effects of realistic surface topography on seismic ground motion in the Yangminshan region of Taiwan based on the spectral-element method and LiDAR DTM, *Bull. seism. Soc. Am.,* **99,** 681–693.

Lovati, S., Bakavoli, M.K.H., Massa, M., Ferretti, G., Pacor, F., Paolucci, R., Haghshenas, E. & Kamalian, M., 2011. Estimation of topographical effects at Narni ridge (Central Italy): comparisons between experimental results and numerical modeling, *Bull. Earthq. Eng.,* **9,** 1987–2005.

Marano, K.D., Wald, D.J. & Allen, T.I., 2010. Global earthquake casualties due to secondary effects: a quantitative analysis for improving rapid loss analyses, *Nat. Hazards,* **52,** 319–328.

Massa, M., Lovati, S., D'Alema, E., Ferretti, G. & Bakavoli, M., 2010. An experimental approach for estimating seismic amplification effects at the top of a ridge, and the implication for ground-motion predictions: the case of Narni (central Italy), *Bull. seism. Soc. Am.,* **100,** 3020–3034.

Maufroy, E., Cruz-Atienza, V.M. & Gaffet, S., 2012. A robust method for assessing 3-D topographic site effects: a case study at the LSBB Underground Laboratory, France, *Earthq. Spectra,* **28,** 1097–1115.

McCrink, T.P., Willis, C.J., Real, C.R. & Manson, M.W., 2010. Effects of topographic position and geology on shaking damage to residential wood-framed structures during the 2003 San Simeon Earthquake, Western San Luis Obispo County, California, *Earthq. Spectra,* **26,** 779–802.

Moczo, P., Bystricky, E., Kristek, J., Carcione, J.M. & Bouchon, M., 1997. Hybrid modelling of P-SV seismic motion at inhomogeneous viscoelastic topographic structures, *Bull. seism. Soc. Am.,* **87,** 1305–1323.

Moore, J.R., Gischig, V., Burjánek, J., Loew, S. & Fäh, D., 2011. Site effects in unstable rock slopes: dynamic behavior of the Randa instability (Switzerland), *Bull. seism. Soc. Am.,* **101,** 3110–3116.

Panzera, F., Lombardo, G. & Rigano, R., 2011. Evidence of topographic effects through the analysis of ambient noise measurements, *Seismol. Res. Lett.,* **82,** 413–419.

Paolucci, R., 2002. Amplification of earthquake ground motion by steep topographic irregularities, *Earthq. Eng. Struct. Dyn.,* **31,** 1831–1853.

Paolucci, R., Faccioli, E. & Maggio, F., 1999. 3D response analysis of an instrumented hill at Matsuzaki, Japan, by a spectral method, *J. Seism.,* **3,** 191–209.

Pischiutta, M., Cultrera, G., Caserta, A., Luzi, L. & Rovelli, A., 2010. Topographic effects on the hill of Nocera Umbra, central Italy, *Geophys. J. Int.,* **182,** 977–987.

Pischiutta, M., Rovelli, A., Vannoli, P. & Calderoni, G., 2011. Recurrence of horizontal amplification at rock sites: a test using H/V based ground motion prediction equations, in *Proceedings of the 4th IASPEI/IAEE International Symposium: Effects of Surface Geology on Seismic Motion,* In CD, University of California Santa Barbara, CA.

Poggi, V., Edwards, B. & Fäh, D., 2011. Derivation of a reference shear-wave velocity model from empirical site amplification, *Bull. seism. Soc. Am.,* **101,** 258–274.

Poggi, V., Edwards, B. & Fäh, D., 2013. Reference S-wave velocity profile and attenuation models for ground-motion prediction equations: application to Japan, *Bull. seism. Soc. Am.,* **103,** 2645–2656.

Roten, D., Cornou, C., Fäh, D. & Giardini, D., 2006. 2D resonances in Alpine valleys identified from ambient vibration wavefields, *Geophys. J. Int.,* **165,** 889–905.

Sepúlveda, S.A., Murphy, W., Jibson, R.W. & Petley, D.N., 2005. Seismically induced rock slope failures resulting from topographic amplification of strong ground motions: the case of Pacoima Canyon, California, *Eng. Geol.,* **80,** 336–348.

Shakal, A., Huang, M. & Cat, T., 1988. The Whittier Narrows, California, earthquake of October 1, 1987: CSMIP strong motion data, *Earthq. Spectra,* **4,** 75–100.

Spudich, P., Hellweg, M. & Lee, W.H.K., 1996. Directional topographic site response at Tarzana observed in aftershocks of the 1994 Northridge, California, earthquake: implications for mainshock motions, *Bull. seism. Soc. Am.,* **86,** S193–S208.

Tucker, B.E., King, J.L., Hatzfeld, D. & Nersesov, I.L., 1984. Observations of hard rock site effects, *Bull. seism. Soc. Am.,* **74,** 121–136.

Turcotte, D.L., 1997. *Fractals and Chaos in Geology and Geophysics,* 2nd edn, Cambridge Univ. Press.

Vidale, J.E., 1986. Complex polarisation analysis of particle motion, *Bull. seism. Soc. Am.,* **76,** 1393–1405.

Weiss, A., 2001. Topographic position and landforms analysis, Poster presentation, in *Proceedings of ESRI User Conference,* San Diego, CA. Available at: http://www.jennessent.com/downloads/tpi-poster-tnc_1822.pdf, last accessed 11 June 2013.

SUPPORTING INFORMATION

Additional Supporting Information may be found in the online version of this article:

Appendix S1. Results for all sites analysed in this study (http://gji.oxfordjournals.org/lookup/suppl/doi:10.1093/gji/ggu014/-/DC1)

Please note: Oxford University Press is not responsible for the content or functionality of any supporting materials supplied by the authors. Any queries (other than missing material) should be directed to the corresponding author for the article.